Eur. Phys. J. E (2014) **37**: 57
DOI 10.1140/epje/i2014-14057-6

THE EUROPEAN PHYSICAL JOURNAL E

Regular Article

Role of hydrophobicity on interfacial fluid flow: Theory and some applications

B. Lorenz[1,2], N. Rodriguez[3], P. Mangiagalli[4], and B.N.J. Persson[1,2,a]

[1] PGI, FZ-Jülich, D-52425 Jülich, Germany
[2] Multiscale Consulting, Victor Gollancz Str. 50, 52428 Jülich, Germany
[3] BD Medical-Pharmaceutical Systems, 1 Becton Drive, Franklin Lakes, NJ 07417, USA
[4] BD-Pharmaceutical Systems, 11 Rue Aristide BERGES-B. P. 4, 38800 Pont de Claix, France

Received 28 January 2014 and Received in final form 7 April 2014
Published online: 27 June 2014 –

Abstract. The fluid flow through a seal interface depends on the percolating non-contact channels morphology, size and length, and on the interfacial surface energies. In particular, hydrophobic interfaces may expel fluids and decrease the fluid flow of seals, while increasing the sliding friction. We present results of interfacial fluid flow experiments on a hydrostatic column device which demonstrate how interfacial hydrophobicity can block fluid flow at interfaces and reduce the leak rate of seals. The presented results may help to understand the role of interfacial hydrophobicity in many practical applications, some of which we discuss briefly in this paper, *e.g.*, rubber wiper blades on hydrophobic (usually wax-coated) glass, the locomotion of insects on surfaces in water, and syringes.

1 Introduction

A seal is a device for closing a gap or making a joint fluid tight satisfying certain functional requirements. In this sense, a seal may or may not be considered as such depending of the application. For example, a rubber gasket or a rubber O-ring may act as perfect seals in many applications, like a hydraulic piston, but due to the permeability of the rubber to several gases it is not a seal in a ESCA (Electron Spectroscopy for Chemical Analysis) instrument where high vacuum is required. Another example is in the pharmaceutical industry where breathable membranes and rubbers are used to seal sterile devices while allowing the permeation of the sterilization gas, *e.g.*, ethylene oxide and steam. Therefore, the notion of seal is intimately related to some functional criteria which depend of the field of application.

In spite of its apparent simplicity, it is not easy to predict the leak rate and (for dynamic seals) the friction forces [1]. The main problem is the influence of surface roughness on the contact mechanics at the seal-substrate interface. Most surfaces of engineering interest have surface roughness on a wide range of length scales [2], *e.g.*, from cm to nm, which will influence the leak rate and friction of seals.

We have recently presented experimental results for the leak rate of rubber seals [3–5], and compared the results to a "critical-junction" theory [2, 6, 7], which is based on percolation theory and a contact mechanics theory [8–14]. We have also used a more accurate effective medium theory, which takes into account all the fluid flow channels in an approximate way. However, the obtained results are very similar to those of the critical-junction theory.

In most applications of seals the fluid wets the solid walls (hydrophilic system) and one expects the fluid to fill out all pores or channels at the interface, at least for a stationary seal. Here we will discuss how hydrophobicity will affect the leak rate of seals, and we present results of leak rate experiments which demonstrate how air bubbles trapped at the interface as a result of interfacial hydrophobicity can block fluid flow at interfaces and reduce the leak rate of seals. The presented results help to understand the role of interfacial hydrophobicity in many practical applications, *e.g.*, the action of rubber wiper blades on hydrophobic (usually wax-coated) glass, leak rate in syringes, or locomotion and adhesion of insects to surfaces in water.

2 leak rate theory

We first briefly review the leak rate model developed in refs. [2, 6, 7]. Consider the fluid leakage through a stationary rubber seal, from a high fluid pressure p_a region, to a low fluid pressure p_b region. Assume that the nominal

[a] e-mail: b.persson@fz-juelich.de

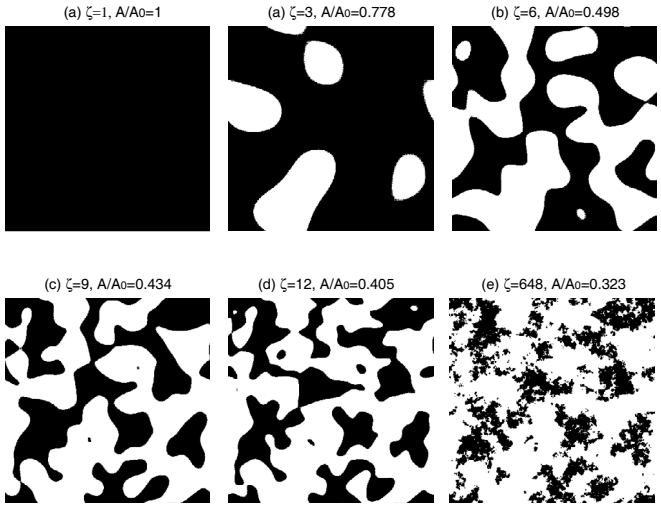

Fig. 1. The contact between two elastic solids with randomly rough (self-affine fractal) surface roughness. The interface is studied at different magnification. At low magnification no surface roughness is observed and it appears as if the contact between the solids is complete. As the magnification increases surface roughness is observed and some non-contact areas can be detected. At high enough magnification, say $\zeta = \zeta_c$, the non-contact area percolates for the first time. The narrowest constrictions in the percolating non-contact channel are denoted as critical constrictions. Adapted from [7].

contact region between the rubber and the hard counter surface is a square with area $L \times L$. We assume that the high-pressure fluid region is for $x < 0$ and the low-pressure region for $x > L$. Now, let us study the contact between the two solids as we increase the magnification ζ. We define $\zeta = L/\lambda$, where λ is the resolution, and study how the apparent contact area (projected on the xy-plane), $A(\zeta)$, between the two solids depends on the magnification ζ. At the lowest magnification we cannot observe any surface roughness, and the contact between the solids appears to be complete $A(1) = A_0$ (see fig. 1(a)). As we increase the magnification we will observe some interfacial roughness, and the (apparent) contact area will decrease. At high enough magnification, say $\zeta = \zeta_c$, a percolating path of non-contact area will be observed for the first time, see fig. 1(d). We denote the narrowest constriction along this percolation path as the *critical constriction*. The critical constriction will have a lateral size $\lambda_c = L/\zeta_c$ and a surface separation u_c at this point. We can calculate u_c using a contact mechanics theory [13]. As we continue to increase the magnification we will find more percolating channels between the surfaces, but these will have more narrow constrictions than the first channel which appears at $\zeta = \zeta_c$, and as a first approximation one may neglect the contribution to the leak rate from these channels [7].

A first rough estimate of the leak rate is obtained by assuming that all the leakage occurs through the critical percolation channel, and that the whole pressure drop $\Delta p = p_a - p_b$ (where p_a and p_b is the pressure to the left and right of the seal) occurs over the critical constriction (of width and length $\lambda_c \approx L/\zeta_c$ and height u_c). We will refer to this theory as the "critical-junction" theory. If we approximate the critical constriction as a pore with rectangular cross-section (width and length λ_c and height $u_c \ll \lambda_c$), and assume an incompressible Newtonian fluid, the volume-flow per unit time through the critical constriction will be given by (Poiseuille flow)

$$\dot{Q} = \frac{u_c^3}{12\eta}\Delta p, \tag{1}$$

where η is the fluid viscosity. In deriving (1) we have assumed laminar flow and that $u_c \ll \lambda_c$, which is always satisfied in practice.

To complete the theory we must calculate the separation u_c of the surfaces at the critical constriction. We first determine the critical magnification ζ_c by assuming that the apparent relative contact area at this point is given by site percolation theory. Thus, the relative contact area $A(\zeta)/A_0 \approx 1 - p_c$, where p_c is the so-called percolation threshold [15]. We take $p_c \approx 0.6$ so that $A(\zeta_c)/A_0 \approx 0.4$ will determine the critical magnification $\zeta = \zeta_c$. The (apparent) relative contact area $A(\zeta)/A_0$ at the magnification ζ can be obtained using the contact mechanics formalism developed elsewhere [8–13], where the system is studied at different magnifications ζ. This theory also determines the separation u_c between the surfaces at the critical constriction.

We note that the calculation of leak rates using the critical junction theory presents a very quick, small-effort estimation of the leak rate. In addition it gives an estimation of the surface separation at the critical junction which is important for understanding several related problems such as the clogging of the flow channels by particles (which often occur in engineering applications), or the container closure integrity for syringes (no prion, virus or bacteria should be able to penetrate into the syringe fluid). We have not compared the size of the critical junction to the results of exact numerical simulations (which would be an interesting research project), but have indirect tests where calculated leak rates have been compared successfully to experimental data and to the effective medium theory prediction (see also ref. [15] where the effective medium theory was compared to exact numerical data).

The picture presented above assumes that the narrowest constriction of the first percolating channel (observed with increasing magnification) can be used to estimate the leak rate. This assumes that the narrowest constrictions of all subsequently opened channels would be smaller, as they stem from smaller-wavelength roughness. While the argument is plausible, it is quite easily conceivable that subsequently added roughness closes the existing channel, or that the original constriction is opened wider. While these effects should be studied in greater detail, we note that the effective medium theory, when applied to the present problem, gives similar leak rate results as the critical-junction theory. In the effective medium theory all leak rate channels (small and big) are included in an approximate way.

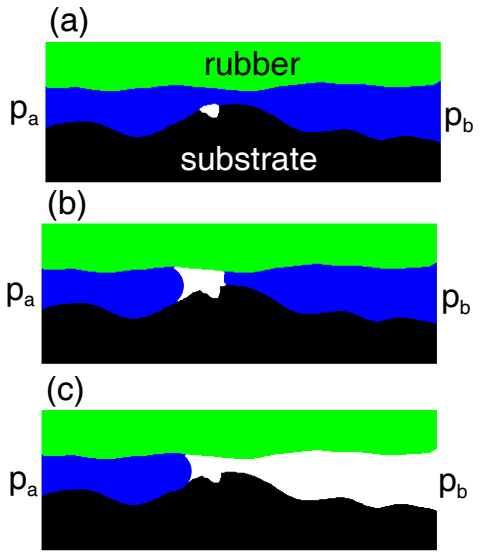

Fig. 2. For a hydrophobic interface the growth of an air bubble trapped in a cavity may result in blocking the fluid flow channels and to a reduction in the leak rate with increasing time of contact.

3 Fluid flow at hydrophobic interfaces

The fluid pressure necessary to squeeze a fluid through a pore of height u and lateral size $\lambda_x \gg u$ and $\lambda_y \gg u$ is given by the Laplace pressure

$$p = \frac{\gamma}{r} = -(\cos\theta_0 + \cos\theta_1)\frac{\gamma}{u}\,, \tag{2}$$

where γ is the surface tension of the fluid and r the radius of curvature of the fluid surface in the pore, and θ_0 and θ_1 are the contact angles on the surfaces of the top and bottom solids. Thus, in the critical-junction theory, if the critical junction has height u_c no leakage will be observed if the fluid pressure difference $\Delta p = p_a - p_b$ between the two sides is less than the *expel pressure* p_e given by (see fig. 2)

$$p_e = -(\cos\theta_0 + \cos\theta_1)\frac{\gamma}{u_c}\,. \tag{3}$$

We denote by hydrophobic interface the case when $\cos\theta_0 + \cos\theta_1 < 0$ and otherwise the interface is referred to as hydrophilic. Note that if an interface is hydrophobic or hydrophilic depends on the solids and the fluid involved in the particular case under study. Interfacial hydrophobicity can be taken into account in the more accurate effective medium theory of interfacial fluid flow in the following way: In the effective medium theory enters the distribution of interfacial separations $P(u)$ which has a delta function $(A/A_0)\delta(u)$ at $u = 0$ with a weight A/A_0 given by the contact area. Note that $P(u)$ is normalized so that

$$\int_{0^-}^{\infty} \mathrm{d}u\; P(u) = 1. \tag{4}$$

To take into account hydrophobicity we replace in the effective medium theory $P(u)$ with $\tilde{P}(u)$ defined by $\tilde{P}(u) = P(u)$ for $u > u_c(p_{\rm fluid})$, and $\tilde{P}(u) = 0$ for $0^+ < u < u_c(p_{\rm fluid})$, and with the weight $\tilde{A}/A_0$ of the delta function at $u = 0$:

$$\frac{\tilde{A}}{A_0} = \frac{A}{A_0} + \int_{0^+}^{u_c(p_{\rm fluid})} \mathrm{d}u\; P(u).$$

Note that $\tilde{P}(u)$ also satisfies the normalization condition (4). In the equations above

$$u_c(p_{\rm fluid}) = -(\cos\theta_0 + \cos\theta_1)\frac{\gamma}{p_{\rm fluid}}\,. \tag{5}$$

This theory can also be applied to lubricated sliding dynamics. Thus the fluid pressure and shear flow factors, which enter in the effective thin-film fluid flow equations, can be calculated approximately using the same effective medium theory description as used for the leak rate calculations. It is easy to estimate under which condition hydrophobicity will be important in mixed lubrication. The fluid pressure at the sliding interface (assuming the fluid penetrates the sliding junction) is of order $p_{\rm fluid} \approx \alpha\eta v_0 L/u_0^2$, where η is the fluid viscosity, v_0 the sliding speed, u_0 a typical interfacial separation, L the width of the Hertzian contact region and $\alpha \approx 0.2$. This expression for $p_{\rm fluid}$ assumes that the sliding interface is nearly flat and slightly tilted (with the ratio between the surface separations at the inlet and outlet of the contact of order 1.5 as found in experiments and calculations). Thus if

$$\frac{\alpha\eta v_0 L}{u_0^2} < -(\cos\theta_0 + \cos\theta_1)\frac{\gamma}{u_c}\,,$$

or if $u_0 \approx u_c$

$$v_0 < -(\cos\theta_0 + \cos\theta_1)\frac{5\gamma u_c}{\eta L}\,, \tag{6}$$

the hydrophobicity will have a strong influence on the fluid flow and friction of the sliding junction. For a rubber wiper blade sliding on wet (water, *e.g.*, during raining) wax-coated glass we have typically $L \approx 0.2\,\mathrm{mm}$ and $u_c \approx 1\,\mu\mathrm{m}$, and using $\eta = 0.001\,\mathrm{Pa\,s}$ and $\gamma \approx 0.07\,\mathrm{J/m^2}$ the right-hand side of (6) becomes $\approx 1\,\mathrm{m/s}$ which is consistent with experiments where the friction of wet wax-coated glass is much higher than for wet uncoated glass for low velocities (mixed lubrication).

We will denote the pressure necessary to force a liquid through a capillary, or into some more complex shaped volume bounded by hydrophobic surfaces (see sect. 7), as the *expel pressure* p_e. In general, p_e is the product of the fluid surface tension γ, the hydrophobicity number $-(\cos\theta_0 + \cos\theta_1)$ and some inverse length which depends on the geometrical shape of the volume between the solids. Using the Young's equation $\gamma\cos\theta = \gamma_{\rm SV} - \gamma_{\rm SL}$ we can write

$$-\gamma(\cos\theta_0 + \cos\theta_1) = (\gamma_{\rm S_0L} + \gamma_{\rm S_1L}) - (\gamma_{\rm S_0V} + \gamma_{\rm S_1V}),$$

where S, L and V stands for solid, liquid and vapor, respectively.

It is important to distinguish between dewetting and interfacial hydrophobicity. A dewetting process [16–19] involves removing the fluid between asperity contact regions leading to dry contact area. Dewetting depends on the sign of the spreading pressure $S = \gamma_{S_0S_1} - \gamma_{S_0L} - \gamma_{S_1L}$. If $S > 0$ the liquid likes to stay between the surfaces (it acts like a lubricant) and is removed only if a large enough external pressure acts at the interface. If $S < 0$ the fluid film is unstable and the asperity contact regions dewet resulting in dry contact regions. In this case an effective (short-ranged) attractive interaction occurs between the surfaces. However, for surfaces with large enough roughness non-contact channels may still prevail and may be filled by the fluid. That is, dewetting does not necessarily imply interfacial hydrophobicity (and vice versa). This is also clear from the fact that the spreading pressure depends on the (dry) wall-wall binding energy (per unit surface area) $\gamma_{S_0S_1}$, while this quantity does not enter in the expel pressure. Similarly the surface energies γ_{S_0V} and γ_{S_1V} enter in the expel pressure, but not in the spreading pressure. However, both quantities depend on γ_{S_0L} and γ_{S_1L}. For solids interacting mainly via the van der Waals interaction one has $\gamma_{S_0S_1} \approx (\gamma_{S_0V}\gamma_{S_0V})^{1/2}$ and in this case it is easy to show that interfacial hydrophobicity imply dewetting, while the opposite is not true in general.

We note that even if dewetting does not occur and the solids in the asperity contact region are separated by a thin (nanometer) fluid (lubrication) film, the sliding friction may still be increased if the interface is hydrophobic when compared to the case of hydrophilic interface. The reason is that at the onset of sliding, in the former case the asperity contact regions slide into dry surface areas, where the friction may be higher than for the lubricated surfaces, while in the latter case the surface separation in the asperity contact regions may even increase due to build up of fluid pressure (elastohydrodynamic at the asperity level).

To summarize, the spreading pressure determines if the contact regions will be dry or separated by a thin (typically a few nanometer thick) fluid film, while the expel pressure determines if the (percolating) non-contact channels will be dry or filled with fluid.

4 Experimental

We have performed a very simple experiment to test the theory presented above. In fig. 3 we show our set-up for measuring the leak rate of seals. A glass (or PMMA) cylinder with a rubber ring (with rectangular cross-section) attached to one end is squeezed against a hard substrate with well-defined surface roughness. The cylinder is filled with water, and the leak rate of the fluid at the rubber-counter surface is detected by the change in the height of the fluid in the cylinder. In this case the pressure difference $\Delta p = p_a - p_b = \rho g h$, where g is the gravitation constant, ρ the fluid density and h the height of the fluid column.

In our study we use a rubber ring with Young's elastic modulus $E = 2.3\,\mathrm{MPa}$, and with inner and outer diameter 3 cm and 4 cm, respectively, and the height 0.5 cm. The rubber ring was made from a silicone elastomer (PDMS) prepared using a two-component kit (Sylgard 184) purchased from Dow Corning (Midland, MI). The kit consists of a base (vinyl-terminated polydimethylsiloxane) and a curing agent (methylhydrosiloxane-dimethylsiloxane copolymer) with a suitable catalyst. From these two components we prepared a mixture 10:1 (base/cross linker) in weight. The mixture was degassed to remove the trapped air induced by stirring from the mixing process and then poured into casts. The bottom of these casts was made from glass to obtain smooth surfaces. The samples were cured in an oven at 80 °C for 12 h.

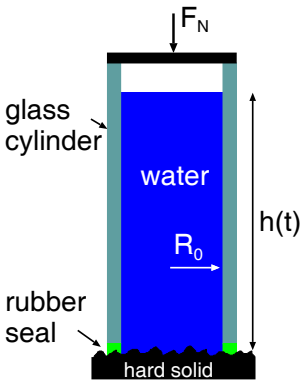

Fig. 3. Experimental set-up for measuring the leak rate of seals. A glass (or PMMA) cylinder with a rubber ring attached to one end is squeezed against a hard substrate with well-defined surface roughness. The cylinder is filled with water, and the leak rate of the water at the rubber-counter surface is detected by the change in the height of the water in the cylinder.

In the present experiments we use sand-blasted glass surfaces as substrates. For untreated glass the rubber-glass interface is hydrophilic with nearly zero water contact angle. We have made the glass surface hydrophobic by exposing it to perfluorooctyltrichlorosilane (FOTCS). These molecules form a grafted monolayer with hydrophobic property. The sample was exposed in such vapor in a vacuum desiccator for an hour under a pressure of 45 mbar. The contact angle values of FOTCS grafted to a flat glass surface is in the range of 105° to 115° (see ref. [20]). On the rough surface the contact angle is even larger. The hydrophobic surface is quite stable and can be used many times. After all the measurements on the hydrophobic surface we have removed the grafted layer (without changing the surface topography) by shortly treating the interface with oxygen plasma. An alternative method is to clean it with piranha solution (a 3:1 mixture of concentrated sulfuric acid ($H_2 2SO_4$) with hydrogen peroxide (H_2O_2)) but this may also (slightly) modify the surface topography and was not used. We have studied the leak rate using the same glass surface with and without the grafted monolayer. Figure 4 shows an example of water droplets formed after a short contact time on the glass surface, resulting from leakage at the interface between the rubber and the

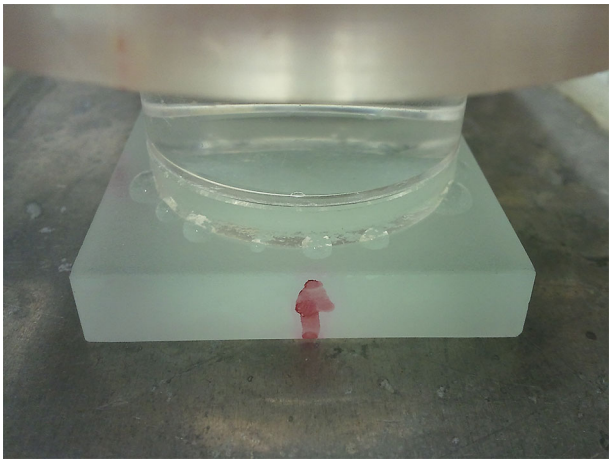

Fig. 4. Fluid drops at the seal-substrate edge after a short leak time with hydrophobic interface (silicone rubber in contact with rough hydrophobic glass).

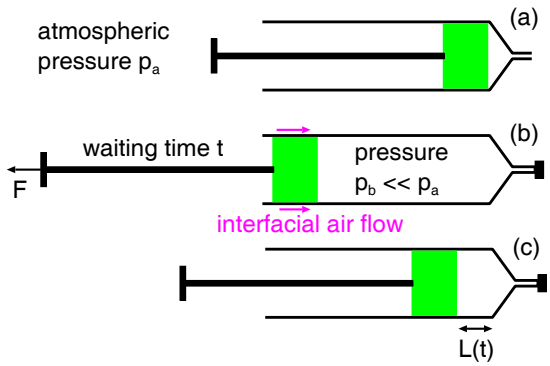

Fig. 5. (a) The barrel-stopper was assembled in empty configuration and the stopper pushed to the end of the barrel, resulting in a very small volume of gas at atmospheric pressure. (b) Next the needle was closed with a rubber plug so no air could penetrate into the syringe from the needle side, and the stopper pulled back (retracted) to full fill position. (c) After waiting some time the pull force was removed, this resulted in the stopper moving to a new position where the pressure force (due to the difference in the gas pressure inside and outside the barrel) is equal to the stopper-barrel friction force.

hydrophobic glass. In all the experiments presented below the nominal rubber-glass contact pressure is $\approx 1\,\mathrm{MPa}$.

We have measured the leakage for experimental syringes using the following procedure (see fig. 5): Experiments were performed with PTFE (Teflon) laminated rubber stoppers in glass and polymer barrels. The barrel-stopper was assembled in empty configuration and the stopper pushed to the end of the barrel, resulting in a very small volume of gas at atmospheric pressure. Next the needle was closed so no air could penetrate into the syringe from the needle side, and the stopper pulled back (retracted) to full fill position. After waiting some time the pull force was removed, which resulted in the stopper moving to a new position where the gas pressure force (due to the difference in the gas pressure inside and outside the barrel) is equal to the stopper-barrel friction force. We estimate the interfacial flow of air (leak rate) by plotting the displacement of the stoppers (from the initial equilibrium position) as a function of waiting time, and applying the ideal gas low for the pressure changes. This is an approximate estimation of the leakage since it does not account for the surface modifications on sliding each time the stopper is actuated neither for any gas permeability contribution from other components of the syringe. From the measured air leak rate one can calculate the water leak rate by taking into account the difference in the viscosity between air and water ($\approx 1.8 \times 10^{-5}\,\mathrm{Pa\,s}$ and $\approx 1.0 \times 10^{-3}\,\mathrm{Pa\,s}$, respectively), and also taking into account that the mean free path l for a molecule in air ($\approx 70\,\mathrm{nm}$) is of similar magnitude as the height u_c of the critical junction (*i.e.* the Knudsen number $K = l/u_c \approx 1$), making it necessary to correct the continuum mechanics theory predictions of the leak rate (see appendix A).

5 Experimental results and analysis

In the critical-junction theory the leak rate of a seal is given by

$$\dot{Q} = \frac{L_y}{L_x}\frac{u_c^3}{12\eta}\Delta p, \tag{7}$$

where Δp is the fluid pressure drop over the seal and η the fluid viscosity. L_x and L_y are the width (in the fluid flow direction) and length (orthogonal to the fluid flow) of the seal and u_c the height of the narrowest pass (denoted critical junction) along the non-contact percolation channel (the first non-contact percolating channel observed as the magnification increases). In order to prevent fluid from flowing through the critical junction, we must have $\Delta p < \gamma/r_c$ where $u_c = -r_c(\cos\theta_1 + \cos\theta_2)$. Thus as Δp decreases the fluid flow will stop when

$$\Delta p = p_e = -(\cos\theta_1 + \cos\theta_2)\gamma/u_c. \tag{8}$$

If $A_w = \pi R_0^2$ is the cross-section area of the water column and $h(t)$ the height (see fig. 3), the water volume $V = hA_w$ must satisfy the equation $A_w\dot{h}(t) = -\dot{Q}$ or

$$\dot{h}(t) = -\dot{Q}/A_w. \tag{9}$$

The pressure of the water at the bottom of the column $\Delta p = \rho g h$. Using (7) we can write

$$\frac{\dot{Q}}{A_w} = \frac{L_y}{L_x}\frac{\rho g u_c^3}{12\eta A_w}h(t) = \alpha(t)h(t), \tag{10}$$

where the leak rate factor

$$\alpha(t) = \frac{L_y}{L_x}\frac{\rho g u_c^3}{12\eta A_w} \tag{11}$$

in general depends on time because of viscoelastic relaxation in the rubber which tends to reduce the interfacial separation with increasing time. In addition there may be clogging of leak channels by contamination particles. For a

hydrophobic interface, nucleation and growth of gas bubbles[1] which can block the leak channels (see fig. 2) may also introduce a time dependency of $\alpha(t)$. Combining (9) and (10) gives

$$\dot{h} = -\alpha(t)h, \tag{12}$$

or

$$\ln\left(\frac{h}{h_0}\right) = -\int_0^t \mathrm{d}t'\ \alpha(t'),$$

where $h_0 = h(0)$ is the height of the water column at time $t = 0$. In fig. 6 we show $\log_{10}[\ln(h/h_0)]$ as a function of $\log_{10} t$ for both hydrophilic (upper curve; pink symbols) and hydrophobic interfaces. We observe large fluctuations in the results for hydrophobic interfaces when the experiment is repeated under nominally identical conditions (green, blue and yellow symbols). This may reflect subtle changes in the distribution of trapped air bubbles in cavities, and also slightly different contact positions or contact conditions between the rubber and the counter surface. The green, red and black square symbols in fig. 6 shows leak rate data after waiting 1 h, 1.5 h and 2.5 h with the rubber seal in contact with the substrate (and surrounded by water with $\Delta p = 0$), respectively, before filling up the water in the Plexiglas tube to its final value $h_0 \approx 1$ m. The other square symbols were obtained after 10 min waiting time.

The dashed lines in fig. 6 have the slope 1 corresponding to $\ln(h/h_0) \sim t$ or a time-independent leak rate factor α. Thus in all cases for short waiting time (10 min), the leak rate factor is approximately constant for short time. We also observe that for the hydrophobic case the leak rate factor approaches zero for long time and the leak rate vanishes at a finite value of the water column height. For the hydrophilic case $\alpha(t)$ also decreases for large time, which we attribute to viscoelastic relaxation of the silicone rubber, which reduces the height of the leak rate channels. In addition some channels may become clogged by contamination particles, since we cannot exclude some low concentration of particles in the water in spite of the fact we use distilled water in the experiments. Since the critical (or narrowest) junctions of the leak channels are very small in the present experiment (of order $\sim 10\,\mu$m) even small contamination particles can clog some channels.

From fig. 6 for the hydrophilic interface the initial linear dependency $\ln(h/h_0) \sim t$ (dashed line) gives the leak rate factor $\alpha \approx (2.85 \pm 0.1) \times 10^{-5}\,\mathrm{s}^{-1}$. Using (11) this gives $u_c \approx 8.8\,\mu$m. For the hydrophobic interface $\theta_0 \approx \theta_1 \approx 125°$ giving $\cos\theta_0 + \cos\theta_1 \approx -1.15$. Using (3) this gives the expel pressure $p_e \approx 8.3$ kPa which corresponds to the pressure at the bottom of an approximately $h = 0.83$ m height water column.

[1] An air bubble is not thermodynamically stable on a flat surface in water independent of if the surface is hydrophobic or hydrophilic. However, an air bubble bridging two hydrophobic surfaces is stable, and for hydrophobic surfaces with surface roughness air bubbles may be stable in valleys or cavities. The interaction between hydrophobic surfaces in water is not well understood and still a controversial topic, see, *e.g.* [21]

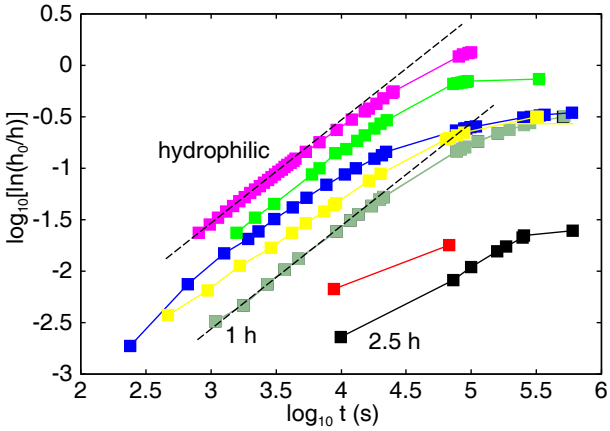

Fig. 6. The height of the water column $h(t)$ as a function of time t. The dashed lines have the slope 1 corresponding to $\ln(h/h_0) \sim t$ or a time-independent leak rate factor α. The pink symbols are for hydrophilic interface and all other symbols for hydrophobic interfaces. The pink, green, blue and yellow symbols are for waiting time 10 min with the rubber seal in contact with the substrate (and surrounded by water with $\Delta p = 0$) before filling up the water in the plexiglas tube to its final value $h_0 \approx 1$ m. The green red and block curves are for the waiting time 1, 1.5 and 2.5 h, respectively.

In our experiment with hydrophobic surfaces we first bring the rubber seal in contact with the substrate in the presence of water. If in the initial state water had not filled all the non-contact regions at the rubber-substrate interface then there should be no difference in the initial leak rate between the hydrophobic and the hydrophilic interface. However, we always observe a clear reduction in the leak rate for the hydrophobic surfaces, see fig. 6, which indicates that some leak rate channels get blocked by air bubbles almost immediately after contact formation. This may be caused by local dewetting processes, *e.g.*, air dissolved in the water may nucleate air bubbles at the interface or, more likely, air may already exist in (deep enough) valleys of the rough substrate profile. Small air bubbles may grow by diffusion of air molecules dissolved in the water to the bubbles. Thus the air bubbles grow with increasing time and may finally block flow channels at the interface. Note that in several cases $\ln(h/h_0) \sim t$ for $t < t_0$ with $t_0 \approx 10^4$ s or ~ 3 h, which shows that the leak rate factor is time independent, at least initially. Thus, during the fluid flow (leakage) no further blocking of flow channels occur for $t < t_0$. This shows that the nucleation and growth of air bubbles may be easier in stationary water than in flowing water as in the latter case small air bubbles may be dragged by the water away from the interfacial region. To test this idea further, we have performed experiments where we wait different time periods before filling the tube with water. In the standard experiments we wait 10 minutes before filling the tube, but we did additional measurements where we wait 1 h, 1.5 h, 2 h, 2.5 h and 5 hours before filling the tube with water. As shown in fig. 6 there is a very strong reduction in the leak rate with the waiting time. For the hydrophilic

interface we observe that even after 5 hours waiting time, the viscoelastic relaxation of the rubber has nearly no influence on the leak rate. Thus, the effect we observe for the hydrophobic interface must be due to the formation of air bubbles blocking with increasing time flow channels at the interface, and not due to a reduction in the interfacial surface separation because of viscoelastic creep.

6 Applications

We have shown above that the leak rate of seals depends on if the interface is hydrophilic or hydrophobic with respect to the fluid involved. For hydrophilic interfaces the fluid will fill out all non-contact percolating interfacial channels after a certain time and the seal will leak unless the contact area (at the highest magnification corresponding to atomic resolution) percolates. For hydrophobic interfaces, if the fluid pressure difference $\Delta p = p_a - p_b$ is below some critical value, say p_e, no fluid leakage will occur even if the non-contact area percolates. The expel pressure p_e depends on the surface tension of the fluid, the contact angles on the solid walls, and on the separation u_c between the surfaces at the narrowest constriction in the largest percolating non-contact channel, which is the percolating non-contact channel first observed as the magnification increases (see fig. 1). The theory also shows that in addition to the seal's leak rate dependence on the wetting properties of the seal interface the sliding friction also is impacted since in general dry surfaces will exhibit higher sliding friction as compared to the case where a thin fluid film prevails at the sliding interface.

There are many practical applications which are closely related to the study above, and here we consider a few different applications of the theory.

6.1 Application to syringes

The theory developed above can be used to study the fluid flow between a rubber seal (stopper) and a syringe barrel. At the present there is interest in the pharmaceutical industry to evaluate syringes with rubber stoppers having a thin ($d \approx 10$–$100\,\mu$m) film of PTFE as coating, and no lubricant (*e.g.* silicone oil) present neither on the barrel nor on the stopper surfaces. The main objectives of such approach are: a) to reduce significantly the level of leachables from the stopper's rubber, and b) to avoid interactions of the drug product with silicone oil interfaces, either at the barrel surface, or at silicone oil droplets suspended in the drug product. Some of those interactions are induced protein aggregation and adsorption [22, 23] and protein denaturing due to induced shear at the silicone oil droplet-drug formulation interface [24]. There have been three practical approaches to the strategy above: a) film lamination or coating of the majority of the area of the stopper's interface with the drug product *e.g.*, FluroTec, b) coating (Plasma, CVD, etc.) of the stopper's entire outside area *e.g.*, Omniflex, and c) film lamination of the stopper's entire outside area *e.g.*, Daikyo Crystal Zenith stoppers and the stoppers used in this work. The first approach requires fluid lubrication since the seal is achieved at the rubber-glass or polymer contact instead of in the laminated or coated portion of the stopper. The second approach is challenging due to the compromise between low friction and container closure performance, and frequently requires some lubrication fluid. Finally the third approach as we will discuss below is able to operate with acceptable friction and container closure performance and the use of none or a very low amount of lubricant.

Most syringes at present have barrel and stopper lubricated with silicone oil in order to reduce the friction between the rubber stopper and the glass or polymer (such as polypropylene or poly-cyclolefins) barrel. Although in significant lower amounts, silicone oil is also added to the stoppers in the stopper placement processes as an aid. For lubricated syringes fluid squeeze-out may result in a slow (in time) increase in the area of real contact and the break-loose friction force [25,26]. The higher the viscosity of the silicone oil the slower is the squeeze-out, and the larger the average surface separation will be at any given time. The silicone oil fill the interfacial channels and prevent the drug product to flow through the interface. The higher the viscosity of the silicone oil the larger is this effect. In addition to its lubrication effect, the silicone oil fills also the interfacial channels preventing the drug product to flow through the interface. The higher the viscosity of the silicone oil the larger is the blocking effect; however, the use of silicone oil with higher viscosities than $\sim 15\,$Pa s has significant manufacturing processes challenges.

Uncoated and non-lubricated rubber stoppers exhibit high friction forces against both glass and polymer barrels (friction coefficients $\mu = 1.4$–1.6), rendering such configurations useless as drug delivery applications. On the other hand, non-lubricated PTFE-coated rubber stopper have acceptable friction forces ($\mu = 0.05$–0.2) against both glass or polymers, and does not requiring additional lubrication, and exhibit very low levels of leachables.

PTFE and other films (*e.g.*, UHMWPE or ETFE) used in laminated stoppers have elastic modules 100–1000 times higher than the typical rubbers used in stoppers (2–6 MPa). Thus, the average interfacial separation, resulting from the surface roughness, is much larger for laminated stopper than for the uncoated rubber stopper. Therefore, for laminated rubber stoppers an accurate calculation of the interfacial separations as well as design parameters (contact pressure, geometry, etc.) is particularly important to assure container closure integrity, low weight losses, functional performance, and no microbial ingress during the shelf life and use of the product.

Hydrophobicity also plays a role since the PTFE-coated rubber stopper is hydrophobic and the barrel counter surface could vary from hydrophilic (bare glass) to hydrophobic (polymer). For a hydrophobic interface, if the pressure difference Δp is below the critical value $p_e = -(\cos\theta_0 + \cos\theta_1)\gamma/u_c$ (eq. (3)), air bubbles may block the non-contact percolating channels in which case no or negligible fluid leakage would occur. In many drug products in the pharmaceutical industry, the drug formu-

Table 1. Water contact angles on different syringe surfaces.

Material	Water contact angle
glass (barrel)	$< 20°$
polymer (barrel)	95°
rubber (stopper)	105°–115°
PTFE (stopper)	125°

Table 2. Hydrophobicity numbers for water between different surface combinations.

Material combination	$-(\cos\theta_0 + \cos\theta_1)$
glass (barrel) - rubber (stopper)	−0.64
glass (barrel) - PTFE (stopper)	−0.41
polymer (barrel) - rubber (stopper)	0.43
polymer (barrel) - PTFE (stopper)	0.66

Table 3. Expel pressure p_e for water, and water with surfactants, between different surface combinations. We used the surface tensions $\gamma = 0.07\,\mathrm{J/m^2}$ for water and $\gamma = 0.02\,\mathrm{J/m^2}$ for water + surfactant, and in both cases $u_c = 70\,\mathrm{nm}$. A negative p_e means that the fluid wets the interface, *i.e.* it spreads spontaneously and fills all interfacial cavities which are connected to the fluid reservoir by non-contact channels.

Material combination	p_e (water)	p_e (water+surfactant)
glass - rubber	−0.64 MPa	−0.18 MPa
glass - PTFE	−0.41 MPa	−0.12 MPa
polymer - rubber	0.43 MPa	0.12 MPa
polymer - PTFE	0.66 MPa	0.19 MPa

lation contains surfactants which lower the fluid surface tension γ and therefore also the expel pressure p_e. In those cases the pressure drop Δp may be larger than p_e and, if not considered correctly, may compromise container closure integrity.

We now consider the problem discussed above in more detail. Let us first present the water contact angles for some of the materials used for syringes (see table 1). The water contact angle on glass surfaces varies from $\sim 50°$ down to less than 20° (at this point sessile drop measurement becomes unreliable, especially on curved surfaces) depending on the surface cleaning conditions. Typical values for glass syringe barrels with manufacturing cleanliness are $< 20°$. It should be noticed that the relatively high water contact angle on the glass surface prior to contact is representative of a long exposure to hydrocarbon vapors presents in the atmosphere and affects even sterile products due to the permeation of such vapors through the device packaging. The water contact angle on uncoated rubber depends on formulation and surface cleanliness/removal of silicone oil and/or demolding agents, but

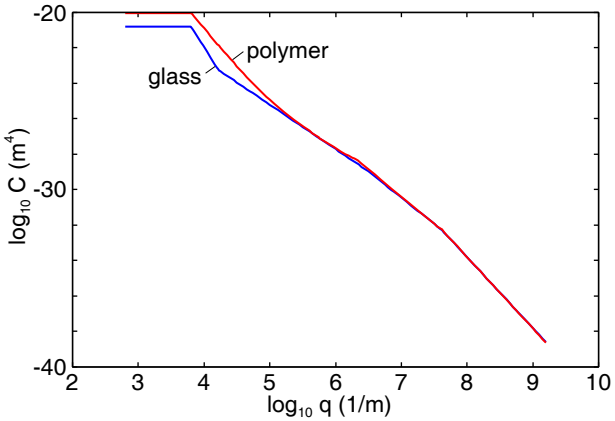

Fig. 7. The surface roughness power spectra of the combined roughness for PTFE-coated rubber stopper against polymer (red) and glass (blue) barrels. The root-mean-square roughness amplitudes are $h_{\mathrm{rms}} = 1.4\,\mu\mathrm{m}$ and $0.5\,\mu\mathrm{m}$, respectively, while the rms slopes are nearly the same (0.68 and 0.67, respectively), since it is dominated by the short-wavelength roughness which are nearly the same for both cases.

varies between 105° and 115°. The water contact angle on the typical polymer barrel surface is around 95°. Water contact angle on rubber surfaces coated with PTFE depends on the process of deposition/lamination, but is typically $\sim 125°$. We have also measured the water contact angle on glass surfaces prior and after a single pass of a PTFE laminated stopper (20 measurements per condition were taken and averaged): before contact $64.6° \pm 1.7°$ and after contact $74.2° \pm 7.5°$. This data agrees with literature on the transfer of PTFE to the counter sliding surface and consequently the water contact angle increases, but not uniformly, since standard deviation also increases.

In table 1 we summarize the measured contact angles and in table 2 the calculated hydrophobicity number $-(\cos\theta_0 + \cos\theta_1)$ for some stopper-barrel combinations. In table 3 we give the expel pressure p_e assuming water (surface tension $\gamma = 0.07\,\mathrm{J/m^2}$) and water+surfactant ($\gamma = 0.02\,\mathrm{J/m^2}$), and using the critical-junction height $u_c = 70\,\mathrm{nm}$. The expel pressure for other u_c can be obtained by scaling $p_e \sim 1/u_c$.

We have calculated the leak rate for PTFE-coated rubber stoppers against glass and polymer barrels. Figure 7 shows the surface roughness power spectra of the combined roughness for PTFE-coated rubber stopper against polymer (red) and glass (blue) barrels. The root-mean-square (rms) roughness amplitudes are $h_{\mathrm{rms}} = 1.4\,\mu\mathrm{m}$ and $0.5\,\mu\mathrm{m}$, respectively, while the rms slopes are nearly the same (0.68 and 0.67, respectively), since it is dominated by the short-wavelength roughness which are nearly the same for both cases. In the calculation of the leak rate we include plastic deformation (as described in ref. [27]) of the PTFE film which will allow the surfaces to approach each other, and hence reduce the leak rate.

Figure 8 shows the calculated (effective medium theory) leak rates assuming the PTFE film thickness $15\,\mu\mathrm{m}$, fluid viscosity (water) $\eta = 0.001\,\mathrm{Pa\,s}$, fluid pressure dif-

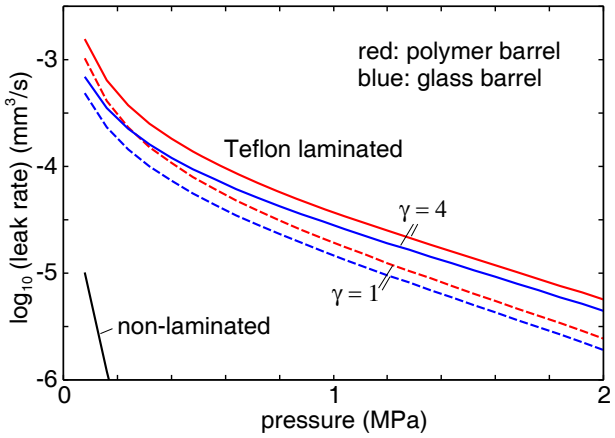

Fig. 8. Calculated leak rate for PTFE-coated rubber stopper against polymer (red) and glass (blue) barrels. We used the PTFE film thickness 15 μm, fluid viscosity (water) $\eta = 0.001$ Pa s, and fluid pressure difference $\Delta p = 0.1$ MPa. Calculations is done for isotropic roughness (Tripp number $\gamma = 1$) (dashed lines), and anisotropic roughness ($\gamma = 4$) (solid lines) with the groves along the syringe axial direction. Also shown (black line) is the calculated leak rate for non-laminated rubber stopper against polymer barrel ($\gamma = 4$) (see also fig. 9).

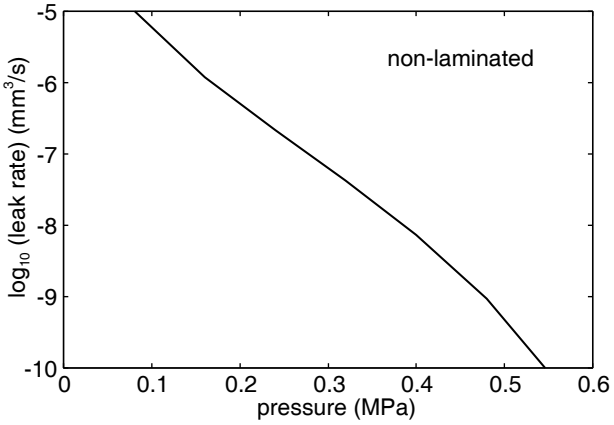

Fig. 9. Calculated leak rate for non-laminated rubber stopper against polymer barrel. We used the fluid viscosity (water) $\eta = 0.001$ Pa s, and fluid pressure difference $\Delta p = 0.1$ MPa. Calculations is done for anisotropic roughness ($\gamma = 4$) with the groves along the syringe axial direction.

ference $\Delta p = 0.1$ MPa, the Tripp number $\gamma = 1$ (dashed curves) and 4 (solid curves). We have used the PTFE elastic modulus $E = 500$ MPa, Poisson ratio $\nu = 0.4$ and penetration hardness $\sigma_Y = 10$ MPa, and for the rubber below the PTFE film, the elastic modulus $E = 4.6$ MPa and Poisson ratio $\nu = 0.5$. For the nominal contact pressure $p_0 = 1$ MPa and assuming $\gamma = 4$, the leak rate for the polymer and glass barrels are 3.4×10^{-5} and 2.6×10^{-5} mm^3/s, respectively. For $\gamma = 1$, the corresponding numbers are 2.1×10^{-5} and 1.6×10^{-5} mm^3/s, respectively. These values are rather close to the experimental value estimated using the very simple approach described in appendix A, which gives $\dot{Q} = (3.4 \pm 1.3) \times 10^{-5}$ mm^3/s for polymer-PTFE laminated stopper syringes when a differential pressure of 0.1 MPa (1 bar) is applied across the stopper. In normal conditions, the stoppers-barrel will not see more than approximately $\Delta p = 0.03$ MPa differential pressure (*e.g.*, during airfreight shipping) therefore the calculated value is an upper bound of the real leak rate.

The theory also predicts[2] that for typical stopper-barrel contact pressure ($p_0 = 1$ MPa) the height of the narrowest constriction along the percolating non-contact channel is about $u_c \approx 50$–70 nm. Taking into account the interfacial hydrophobicity (table 3), for the polymer-PTFE syringes we expect no interfacial fluid flow if the fluid pressure (relative to the atmospheric pressure) is below ≈ 0.6 MPa for water or ≈ 0.2 MPa for water+surfactant with the surface tension 0.02 J/m^2. It is interesting to note that the interfacial separations $u_c \approx 50$–70 nm are smaller than currently considered channel sizes for microbial ingress [28].

With the typical material options (PTFE and UHMW films) in use, the leak rate with laminated stoppers would be larger than for non-laminated stoppers with the same barrel-stopper combined surface roughness, see fig. 9. For the non-laminated rubber stoppers (fig. 9 and black line in fig. 8) the contact area percolates already at the nominal contact pressure $p_0 \approx 0.8$ MPa so for pressures larger than this value no leakage would occur at all. If one includes the adhesional interaction between the surfaces the contact area would percolate for even smaller contact pressures. For PTFE-coated stoppers the adhesion is much less important owing to the much higher elastic modulus of the PTFE as compared to the rubber.

The high coefficient of friction and the adhesion effect in non-lubricated bare rubber stoppers makes it necessary to lubricate the contact (typically using high-viscosity silicone oil) in order to reduce the break-loose (or static) friction so the actuation forces become not too high [25,26]. For the lubricated syringes the contact area becomes smaller and depends on time due to fluid squeeze-out and dewetting [25,26]. This will also result in larger interfacial channels (non-contact), but these channels are now filled with the high viscosity lubrication fluid and may therefore be less problematic from the point of view of drug product leakage and container closure integrity unless microorganisms can diffuse through the fluid (silicone oil) filling the channels. The concept mentioned above is very important because contrary to common assumptions it suggests that

[2] The result in fig. 8 was calculated using the effective medium theory, but we can estimate (from similar calculations with $\gamma = 1$) the separation u_c between the surfaces at the pores where most of the pressure drop occurs using the critical-junction formula $\dot{Q} = (L_y/L_x)u_c^3 \Delta p/(12\eta)$. Thus, using the parameters used in the calculation in fig. 8 (namely $\eta = 0.001$ Pa s, $\Delta p = 0.1$ MPa and $L_y/L_x = 10$) we get $u_c \approx 59$ and 54 nm for the polymer and glass barrel, respectively. If instead the (more approximate) critical-junction theory is used, one obtains $u_c \approx 71$ and 66 nm, respectively. For this small critical-junction one would also expect that clogging by contamination particles in the fluid will have an influence on the time dependency of the leak rate even for hydrophilic junctions.

under the circumstances mentioned above no flow through the interface does not guarantee no-microbial ingress and vice versa the existence of interfacial flow is not a proof that there will be microbial ingress.

In the effective medium theory the region where the fluid cannot exist will percolate and the leak rate will vanish if $\tilde{A}/A_0 > 0.5$ (in a more accurate treatment the contact area will percolate at $A/A_0 = A_c/A_0 \approx 0.42$ and in ref. [29] it was shown how the effective medium approach can be modified to give the correct percolation condition). However, in the effective medium theory the leak rate will be reduced also when Δp is larger than the case where $\tilde{A} = A_c$. This follows from the fact that in the effective medium theory more narrow channels than those observed at the critical magnification will also contribute to the leak rate for hydrophilic interfaces, while for hydrophobic interfaces these smaller channels may get blocked due to the higher Laplace pressure needed to force the fluid through narrow (hydrophobic) channels. It follows that in the effective medium theory the leak rate will decrease in a continuous way as Δp is reduced from a high value towards the critical value where $\tilde{A} = A_c$. However, for real systems close to the critical value of $\tilde{A}/A_0$ one expects large fluctuations in the leak rate as a function of Δp as individual flow channels get blocked as Δp approaches (from above) its critical value where $\tilde{A} = A_c$.

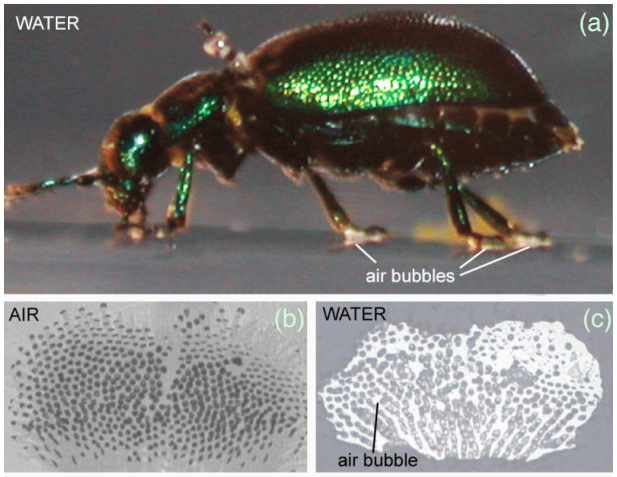

Fig. 10. (a) Beetle walking under water (white lines indicate trapped air bubbles). (b) Contact areas (dark zones) between the plate-like structures at the end of the hairs on the attachment pads of a living beetle attached to an inverted glass substrate in air. (c) Contact areas of the air bubbles (bright zones) trapped on the beetle attachment pads with styrene substrate under water. In both cases (b) (dry surfaces) and (c) (in water) the attachment plates at the end of each hair bind to the substrate surface via capillary adhesion involving small oil drops at the interface between the plates and the substrate. Adapted from [31].

6.2 Wiper blades

The wetting properties of an interface is of crucial importance for wiper blades used to remove water from the glass windows on passenger cars. In this case the sliding velocities involved in a typical case are so high that a thin water film separates the sliding surfaces (mixed lubrication) and the friction is relatively low and not very strongly velocity dependent in the relevant sliding velocity range. This results in stable wiping action. However, recently hydrophobic glass surfaces, *e.g.*, wax-coated glass, are used where water droplets may be removed without any need for wiping them off. However during heavy rain wiping is also necessary for the hydrophobic glass surfaces. In this case the water is expelled from the interface between the wiper blade rubber and the glass surface, at least at the lower sliding velocities close to the turning points of the wiper blades. On the hydrophobic glass surfaces at low sliding velocities the sliding friction is much higher than on the hydrophilic glass surfaces, and the friction decreases much more rapidly with increasing sliding velocity than for hydrophilic glass, resulting in much more severe problems involving stick-slip and noise generation.

The same effect as observed for wiper blades has also been observed in model experiments involving the sliding of silicone rubber balls on hydrophilic and hydrophobic substrates lubricated by water-glycerol mixtures [30]. We note that the wetting properties of the rubber tread block - road interface may be very important for the friction between a tire and a road under wet (*e.g.*, raining) conditions. However, for this case we are not aware of any studies of the relevant interfacial surface energies and fluid contact angles which are needed in order to address if the interface will be dry or wet (at low enough rolling or sliding velocities).

6.3 Adhesion and locomotion of insects on surfaces in water

The removal of fluids at interfaces because of hydrophobicity is also of great importance in some biological attachment systems [31]. Thus, for example, some beetles can walk on surfaces under water. Under dry condition (no water) the beetle binds to surfaces via plate-like structures at the end of the hairs on the attachment pads, see fig. 10(b). Figure 10(a) shows a beetle walking under water where the white lines indicate trapped air bubbles between the beetle attachment pads and the substrate. Figure 10(c) shows the contact areas of the air bubble (bright zones), trapped on the beetle attachment pads, with the styrene substrate under water[3]. The trapped air bubble is not removed even at the water pressure $p_0 \approx 10\,\text{kPa}$ or more, prevailing at a water depth of a few meters. For hydrophobic substrates the adhesion and friction between the beetle attachment pads and the substrate in the dry and wet condition may be of similar magnitude. On strongly hydrophilic substrates in water, a thin water film may separate the attachment

[3] In both cases (b) (dry surfaces) and (c) (in water) the attachment plates at the end of each hair bind to the substrate surface via capillary adhesion involving small oil drops at the interface between the plates and the substrate, but this fact is irrelevant here.

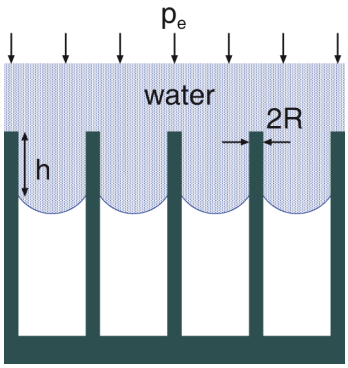

Fig. 11. Water squeezed into an array of hydrophobic fibers (cylinder roads with radius R).

pads from the substrate, resulting in negligible adhesion and friction. Experiments have shown that adding a surfactant to the water removes the air bubbles and results in negligible beetle adhesion under water (the beetle loses its contact with the solid substrate and detaches from the surface) [31].

Let us calculate the expel pressure p_e for the beetle attachment pad (see also refs. [32, 33]). The attachment pad consists of an array of thin fibers. Consider squeezing a fluid into the space between the fibers (see fig. 11). The work to move the water free surface a distance Δh is given by $p_e \Delta V$, where the fluid volume $\Delta V = A\Delta h - N\pi R^2 \Delta h$. Here A is the total area (orthogonal to the fibers) and $N\pi R^2$ the (cross-section) area occupied by the fibers (R is the radius of a fiber, and N the number of fibers). The work $p_e \Delta V$ must equal the change in the interfacial energy which equals

$$p_e \Delta V = N 2\pi R \Delta h \left(\gamma_{SL} - \gamma_{SV}\right),$$

or

$$p_e = \frac{2}{R}\frac{c}{1-c}\left(\gamma_{SL} - \gamma_{SV}\right) = \frac{2}{R}\frac{c}{1-c}(-\gamma\cos\theta),$$

where $c = N\pi R^2/A$. For the beetle $2R \approx 1\,\mu$m and $c \approx 0.1$ and using $\theta = 120^\circ$ gives $p_e \approx 16\,$kPa. Finally we note that some aquatic insects have other body parts covered by a dense array of hydrophobic hair which result in a thin film of air retained under water [32,33]. This enables under water respiration without the need for gills. In addition the trapped air may result in drag reduction as demonstrated in recent fluid flow calculations [34].

7 Summary and conclusions

We have presented results of leak rate experiments where the solid surface energy and water contact angles were modified by grafted monolayers without changing the surface topography. For hydrophobic interfaces we observed a smaller leak rate than for hydrophilic interfaces which we explained by some flow-channels being blocked by air bubbles. We observed strong fluctuations in the leak rate when the experiments were repeated under nominally the same conditions which may reflect subtle changes in the distribution of trapped air bubbles in cavities and also slightly different contact positions or contact conditions between the rubber and the counter surface. For experimental syringe applications we showed that the leak rate of coated stoppers is higher than the one corresponding to uncoated stoppers. In both cases the leak rate is impacted significantly by the surface energies at the interface. We also estimated the interfacial separation (at the critical constriction) in the coated plunger-barrel configuration, and it is below the size which would allow microbial ingress. The theory also predicts that the interfacial gas flow experiments we performed on syringes, cannot be analyzed using the continuum mechanics approximations. Using a rarified gas between two plates approximation produces results fairly close to experimental data. More studies of the leak rate of seals, and extension to include water with surfactants (soap), and wider range of fluid pressures, would contribute to a better understanding of the leak rate for hydrophobic interfaces.

We thank Pinggui Li (PGI-8, FZ-Jülich, Germany) for preparing the hydrophobic (perfluorooctyltrichlorosilane) glass surfaces and N. Hosoda and S.N. Gorb for preparing fig. 10. We thank Kellie Heom (BD-Franklin Lakes, USA), Cynthia Fuentes, and Florent Charlon (BD-Pont de Claix, Fance) for the help on the surface characterization. We thank Kellie Heom, Theresa Bankston, Patrick Begley (BD Franklin Lakes, US) for the help on the experiments and comments on the syringe application.

Appendix A.

We have performed a very simple experiment in order to estimate the leak rate of syringes (see fig. 12). We first assemble the barrel-stopper in empty configuration with the stopper pushed to the end of the barrel, resulting in a small volume V_0 of gas in the syringe at atmospheric pressure. Next the needle is closed so no air can penetrate into the syringe from the needle side, and the stopper is pulled back (retracted) to full fill a position resulting in a volume V_b of gas at low pressure $p_b(0)$. In the first experiment the pull force is immediately removed, which results in the stopper moving to a new position $L(0)$ where the pressure force (due to the difference in the gas pressure outside and inside the barrel) is equal to the stopper-barrel friction force. Next we repeat the experiment except now the stopper is kept in the pulled back (retracted) position for some time t. This results (due to air leakage at the barrel-stopper interface) in an increase in the pressure $p_b(t)$, and when the pull force is removed after some time t the stopper will move to a new position with $L(t) > L(0)$. We now derive an equation for the leak rate, which depends on V_b/V_0, $L(t)/L(0)$ and on the waiting time t.

We base the discussion on the critical-junction theory and consider first the gas flow through a rectangular junction with height u_c and with the width and length

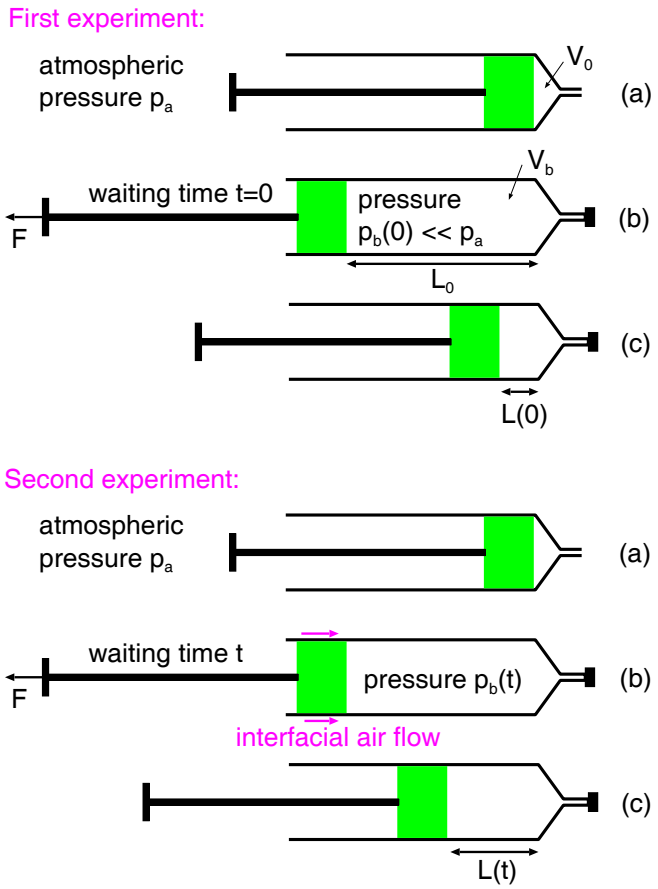

Fig. 12. Experiments performed in order to measure the leak rate of syringes. In the first experiment: (a) The barrel-stopper was assembled in empty configuration and the stopper pushed to the end of the barrel, resulting in a very small volume V_0 of gas at atmospheric pressure. (b) Next the needle was closed so no air could penetrate into the syringe from the needle side, and the stopper pulled back (retracted) to full fill position (gas volume V_b). (c) The pull force is immediately removed, which resulted in the stopper moving to a new position $L(0)$ where the pressure force (due to the difference in the gas pressure inside and outside the barrel) is equal to the stopper-barrel kinetic friction force. The second experiment is the same as the first experiment except now the stopper is kept in the pulled back (retracted) position for some time t. This results (due to air leakage at the barrel-stopper interface) in an increase in the pressure $p_b(t)$, and when the pull force is removed the stopper will move to a new position with $L(t) > L(0)$.

w (see fig. 13). Contact mechanics predicts $w \gg u_\mathrm{c}$. We first assume that we can treat the air as a compressible Newtonian fluid. Introduce a coordinate system with the x-axis along the fluid flow direction and the z-axis in the height direction so the fluid occupy $0 < z < u_\mathrm{c}$. To a good approximation one can consider the gas pressure p and molecular number density n in the junction to depend only on x, *i.e.*, $p \approx p(x)$ and $n \approx n(x)$. In this case the Navier-Stokes equations reduce to a good approximation

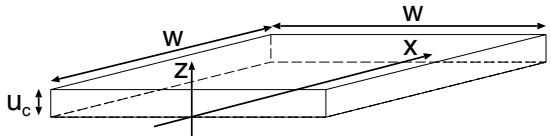

Fig. 13. Critical junction with width and length w and height $u_\mathrm{c} \ll w$.

to

$$\frac{\mathrm{d}p}{\mathrm{d}x} = \eta \frac{\partial^2 v_x}{\partial z^2}\,,$$

where $\eta = \eta_\mathrm{air}$ is the air viscosity (which is independent of the number density n, see footnote [4]). The continuity equation can be written as

$$n(x)\bar{v}_x(x) = \mathrm{const},$$

where

$$\bar{v}_x = \frac{1}{u_\mathrm{c}} \int_0^{u_\mathrm{c}} \mathrm{d}z\; v_x(x,z)$$

is the flow velocity averaged over the height of the gas film. It is easy to solve these equations to obtain the standard result for the flow current $J = n\bar{v}_x$

$$J = \frac{u_c^2}{24 w\eta} \frac{p_a^2 - p_b^2}{k_\mathrm{B}T}\,,$$

where we have used the ideal gas law $p = nk_\mathrm{B}T$. The number of air molecules flowing through the junction per unit time equals $\dot{N} = Jwu_\mathrm{c}$ so that

$$\dot{N} = \frac{u_c^3}{24\eta} \frac{p_a^2 - p_b^2}{k_\mathrm{B}T}\,. \qquad \text{(A.1)}$$

Let $N_\mathrm{b}(t)$ be the number of air molecules in the volume V_b. We get $\mathrm{d}N_\mathrm{b}/\mathrm{d}t = \dot{N}$ or denoting $n_\mathrm{b} = N_\mathrm{b}/V_\mathrm{b}$ and using (A.1)

$$\frac{\mathrm{d}n_\mathrm{b}}{\mathrm{d}t} = \frac{L_y}{L_x} \frac{u_c^3}{24\eta} \frac{p_a^2 - p_b^2}{V_\mathrm{b} k_\mathrm{B}T}\,,$$

where we have also introduced the factor L_y/L_x reflecting the number of percolating channels at the stopper-barrel interface (L_x and L_y are the width (in the fluid flow direction) and length (orthogonal to the fluid flow) of the seal,

[4] It is well known, and also predicted by the kinetic theory of gases, that the viscosity of a dilute gas is independent of the gas density n. Qualitatively it can be understood by considering the shearing of two parallel planes containing a dilute gas in between. If the density of the gas is doubled, there are twice as many molecules available to transport momentum from one plate to the other, but the mean free path l of each molecule is also halved, so that it can transport this momentum only half as effectively. However, this argument is only valid as long as the Knudsen number $K_\mathrm{n} = l/u_\mathrm{c} \ll 1$.

and for syringes typically $L_y/L_x \approx 10$). Using $p_\mathrm{b} = n_\mathrm{b} k_\mathrm{B} T$ we get

$$\frac{\mathrm{d}p_\mathrm{b}}{\mathrm{d}t} = \frac{L_y}{L_x}\frac{u_c^3}{24\eta}\frac{p_a^2 - p_b^2}{V_\mathrm{b}}\,.$$

It is easy to integrate this equation to get

$$p_\mathrm{b}(t) = p_\mathrm{a}\frac{(p_\mathrm{a}+p_\mathrm{b}^o)e^{\kappa t} - (p_\mathrm{a}-p_\mathrm{b}^o)}{(p_\mathrm{a}+p_\mathrm{b}^o)e^{\kappa t} + (p_\mathrm{a}-p_\mathrm{b}^o)}\,, \tag{A.2}$$

where $p_\mathrm{b}^o = p_\mathrm{b}(0)$ is the gas pressure in the volume V_b at time $t = 0$, and where

$$\kappa = \frac{L_y}{L_x}\frac{u_c^3}{12\eta}\frac{p_a}{V_\mathrm{b}}\,. \tag{A.3}$$

Let us now apply this equation to the experiments shown in fig. 12. Let us assume that when the external force F is removed, the stopper stops when the gas pressure in the barrel equals p_b^* at which point the pressure force $(p_\mathrm{a} - p_\mathrm{b}^*)A$ (where A is the stopper cross-section area) equals the stopper-barrel kinetic friction force F_k. Conservation of molecules requires $p_\mathrm{b}(t)L_0 = p_\mathrm{b}^* L(t)$ and $p_\mathrm{b}(0)L_0 = p_\mathrm{b}^* L(0)$ so that

$$\frac{p_\mathrm{b}(t)}{p_\mathrm{b}(0)} = \frac{L(t)}{L(0)}\,.$$

Using (A.2) this gives

$$\frac{L(t)}{L(0)} = \frac{p_\mathrm{a}}{p_\mathrm{b}^o}\frac{(p_\mathrm{a}+p_\mathrm{b}^o)e^{\kappa t} - (p_\mathrm{a}-p_\mathrm{b}^o)}{(p_\mathrm{a}+p_\mathrm{b}^o)e^{\kappa t} + (p_\mathrm{a}-p_\mathrm{b}^o)}\,. \tag{A.4}$$

Let us denote $\beta = p_\mathrm{a}/p_\mathrm{b}(0)$. Using (A.4) we get

$$\kappa = \frac{1}{t}\ln\left(\frac{(\beta-1)(\beta+L(t)/L(0))}{(\beta+1)(\beta-L(t)/L(0))}\right), \tag{A.5}$$

or using (A.3)

$$\frac{L_y}{L_x}\frac{u_c^3}{12\eta}p_a = \frac{V_\mathrm{b}}{t}\ln\left(\frac{(\beta-1)(\beta+L(t)/L(0))}{(\beta+1)(\beta-L(t)/L(0))}\right). \tag{A.6}$$

Note that $p_\mathrm{a}V_0 = p_\mathrm{b}^o V_\mathrm{b}$ so we can write $\beta = V_\mathrm{b}/V_0$. Equation (A.6) can be used to calculate the height u_c of the critical junction from which one can obtain the water leak rate using

$$\dot{Q} = \frac{L_y}{L_x}\frac{u_c^3}{12\eta_\mathrm{water}}\Delta p, \tag{A.7}$$

where η_water is the viscosity of water.

Using the fact that $\beta = V_\mathrm{b}/V_0 \gg 1$ and assuming $L(t)/(\beta L(0)) \ll 1$ one can expand

$$\ln\left(\frac{(\beta-1)(\beta+L(t)/L(0))}{(\beta+1)(\beta-L(t)/L(0))}\right) \approx \frac{2}{\beta}\frac{L(t)-L(0)}{L(0)}\,.$$

In this limiting case (A.6) takes the form

$$\frac{L_y}{L_x}\frac{u_c^3}{12\eta}p_a = \frac{2V_0}{t}\frac{\Delta L}{L(0)}\,, \tag{A.8}$$

where $\Delta L = L(t) - L(0)$. The water leak rate at the pressure difference $\Delta p = p_\mathrm{a} \approx 0.1\,\mathrm{MPa}$ can be obtained from (A.7) and (A.8)

$$\dot{Q} = \frac{\eta_\mathrm{air}}{\eta_\mathrm{water}}\frac{2V_0}{t}\frac{\Delta L}{L(0)} = \frac{\eta_\mathrm{air}}{\eta_\mathrm{water}}\frac{2V_0}{t}\frac{\Delta V}{AL(0)}\,, \tag{A.9}$$

where $\Delta V = A\Delta L$ is the volume change (A is the barrel inner cross-section area).

In the study above we have assumed that air can be treated as a Newtonian fluid. This is only the case as long as the gap height u_c is much larger than the mean free path l for an air molecule. In the present application this is not a good approximation since the mean free path for an air molecule at atmospheric pressure $l \approx 70\,\mathrm{nm}$ while the gap $u_\mathrm{c} \approx 54$–$59\,\mathrm{nm}$. Thus in the present case the (inlet) *Knudsen number* $K_\mathrm{n} = l/u_\mathrm{c} \approx 1$. Strictly speaking, fluid flow for $K_\mathrm{n} > 1$ cannot be described by standard continuum mechanics but require a molecular approach, *e.g.*, molecular dynamics, the kinetic Monte Carlo method, or the Boltzmann equation [35]. However, it has recently been suggested that one may still use (approximately) the Navier-Stokes continuum mechanics approach but with an effective (reduced) viscosity which depends on the Knudsen number and hence on the local gas density n (since the gas mean free path depends on n) [36,37]. The basic idea is that fluid viscosity η reflects the momentum exchange between the fluid molecules, and for an ideal gas η is proportional to the mean free path l. As the fluid is confined between narrowly spaced solid walls, the mean free path of all the molecules will be reduced due to collision with the walls. This effect can be built into the viscosity in an approximative way [38]. However, in addition to a modified (reduced) viscosity it is necessary to change the fluid flow boundary conditions at the solid walls and include slip.

Here we will take a different approach directly based on experimental results for flow of rarefied gases between two parallel surfaces. Roberts [39] has studied the flow of different gases from a high pressure region to a (nearly) vacuum region through a rectangular pore with the width w and length L, with the surface separation $h \ll w$ and $h \ll L$. He found that the leak rate is proportional to w/L as also predicted for the flow of a viscous fluid in the $K_\mathrm{n} \ll 1$ limit. The leak rate was found to depend only on w/L and on the Knudson number at the inlet (high gas pressure side), which we denote by K_n^o, and on h and Δp. The experimental data for a wide range of (inlet) Knudsen numbers $0.06 < K_\mathrm{n}^o < 5$ and for many different gases could be well fitted by an equation which depends on a universal function $f(K_\mathrm{n}^o)$ (see eq. (6) in ref. [39]). For the range of K_n^o values which is of interest for us here (say $0.5 < K_\mathrm{n}^o < 2$) one has to a good approximation $f(K_\mathrm{n}^o) \approx 0.5K_\mathrm{n}^o$ (see fig. 7(a) in ref. [39] and note that $\alpha = 1/K_\mathrm{n}^o$). Using this result and eq. (6) in ref. [39] one can show that the leak rate derived above for a viscous gas still holds but with the gas viscosity η_0 replaced by an effective viscosity

$$\bar{\eta} = \frac{1}{12}\left(\frac{2}{3\pi}\right)^{1/2}\eta_0 \approx 0.04\eta_0.$$

Table 4. The calculated leak rates for water/polymer barrel, with $\eta_{\rm air}$ replaced by $0.04\eta_{\rm air}$ (see text), and with $V_0 = 60\,{\rm mm}^3$, the waiting time $t = 303\,{\rm s}$ and $AL(0) = 100\,{\rm mm}^3$. The leak rate was obtained using (A.9) with the measured volume changes $\Delta V = A\Delta L$ given in the table. The average leak rate $\dot{Q} = (3.4 \pm 1.3) \times 10^{-5}\,{\rm mm}^3/{\rm s}$.

Sample	ΔV (mm^3)	Water leak rate (mm^3/s)
1	12.35	3.5×10^{-5}
1	9.26	2.6×10^{-5}
1	9.26	2.6×10^{-5}
2	9.26	2.6×10^{-5}
2	3.09	0.9×10^{-5}
2	9.26	2.6×10^{-5}
3	18.52	5.3×10^{-5}
3	15.43	4.4×10^{-5}
3	15.43	4.4×10^{-5}

In the present case $K_{\rm n}^o \approx 1.2$ and we will use $\bar{\eta}_{\rm air} \approx 0.04\eta_{\rm air}$. Thus, in the equations above, we must replace $\eta = \eta_{\rm air}$ with $\bar{\eta}_{\rm air} = 0.04\eta_{\rm air}$, and the factor $\eta_{\rm air}/\eta_{\rm water}$ in (A.9) becomes $\bar{\eta}_{\rm air}/\eta_{\rm water} \approx 7.2 \times 10^{-4}$ (where we used $\eta_{\rm air} = 1.8 \times 10^{-5}\,{\rm Pa\,s}$ and $\eta_{\rm water} = 1.0 \times 10^{-3}\,{\rm Pa\,s}$). In table 4 we show the calculated leak rates for water/polymer barrel using (A.9). The average leak rate $\dot{Q} = (3.2 \pm 1.3) \times 10^{-5}\,{\rm mm}^3/{\rm s}$ is rather close to what is predicted theoretically (see sect. 6): for the nominal contact pressure $p_0 = 1\,{\rm MPa}$ and assuming $\gamma = 4$, the leak rate for the polymer and glass barrels are 3.4×10^{-5} and $2.6 \times 10^{-5}\,{\rm mm}^3/{\rm s}$, respectively. Note also that the leak rate depends rather weakly on the time t, *e.g.*, for sample 2 increasing the waiting time t with a factor of ≈ 8 increases the leak rate only by a factor of ≈ 1.15.

According to the theory, the leak rate should be independent of the waiting time but in reality the contact mechanics may depend on the waiting time due to, among others: a) factors increasing the contact area or reducing the surface separation *e.g.*, thermally activated creep (which could influence both $u_{\rm c}$ and the stopper-barrel kinetic friction force) which will increase the contact area or adhesion, and b) contamination *e.g.*, clogging of flow channels by dust particles or formulation aggregates. As regards the later observation, we can mention that the theory predicts a critical constriction in the order of 50–70 nm which is within the range of advanced membrane filtration systems, *e.g.*, Biofil TM II Polyethersulphone Membrane Cartridges.

References

1. M. Mofidi, B. Prakash, B.N.J. Persson, O. Albohr, J. Phys.: Condens. Matter **20**, 085223 (2008).
2. B.N.J. Persson, O. Albohr, U. Tartaglino, A.I. Volokitin, E. Tosatti, J. Phys.: Condens. Matter **17**, R1 (2005).
3. B. Lorenz, B.N.J. Persson, EPL **86**, 44006 (2009).
4. B. Lorenz, B.N.J. Persson, EPL **90**, 38002 (2010).
5. B. Lorenz, B.N.J. Persson, Eur. Phys. J. E **31**, 159 (2010).
6. B.N.J. Persson, O. Albohr, C. Creton, V. Peveri, J. Chem. Phys. **120**, 8779 (2004).
7. B.N.J. Persson, C. Yang, J. Phys.: Condens. Matter **20**, 315011 (2008).
8. B.N.J. Persson, J. Chem. Phys. **115**, 3840 (2001).
9. B.N.J. Persson, Phys. Rev. Lett. **99**, 125502 (2007).
10. B.N.J. Persson, Surf. Sci. Rep. **61**, 201 (2006).
11. B.N.J. Persson, Eur. Phys. J. E **8**, 385 (2002).
12. B.N.J. Persson, F. Bucher, B. Chiaia, Phys. Rev. B **65**, 184106 (2002).
13. C. Yang, B.N.J. Persson, J. Phys.: Condens. Matter **20**, 215214 (2008).
14. B.N.J. Persson, J. Phys.: Condens. Matter **20**, 312001 (2008).
15. W.B. Dapp, A. Luecke, B.N.J. Persson, M. Müser, Phys. Rev. Lett. **108**, 244301 (2012).
16. F. Brochard-Wyart, P.G. de Gennes, J. Phys. C **6**, A9 (1994).
17. P. Martin, F. Brochard-Wyart, Phys. Rev. Lett. **80**, 3296 (1998).
18. B.N.J. Persson, A.I. Volokitin, E. Tosatti, Eur. Phys. J. E **11**, 409 (2003).
19. B.N.J. Persson, E. Mugele, J. Phys.: Condens. Matter **16**, R295 (2004).
20. A. Hozumi, K. Ushiyama, H. Sugimura, O. Takai, Langmuir **15**, 7600 (1995).
21. J. Israelachvili, *Intermolecular Surface Forces*, third edition (Academic Press, 2011).
22. N. Dixit, *Investigation of Factorsffecting Protein=Silicone Oil Interactions*, Ph. D. Thesis, University of Conneticut, USA (2013).
23. J.L. Li, S. Pinnamaneni, Y. Quan, A. Jaiswal, F.I. Andersson, X. Zhang, Pharm. Res. **29**, 1689 (2012).
24. C.R. Thomas, D. Geer, Biotechnol. Lett. **33**, 443 (2010).
25. B.N.J. Persson, N. Prodanov, B.A. Krick, N. Rodriguez, N. Mulakaluri, W.G. Sawyer, P. Mangiagalli, Eur. Phys. J. E **35**, 5 (2012).
26. B. Lorenz, B.A. Krick, N. Rodriguez, W.G. Sawyer, P. Mangiagalli, B.N.J. Persson, J. Phys.: Condens. Matter **25**, 445013 (2013).
27. B.N.J. Persson, B. Lorenz, A.I. Volokitin, Eur. Phys. J. E **31**, 3 (2010) (see sect. 5).
28. L.E. Kirsch, PDA J. Pharm. Sci. Technol. **54**, 305 (2000).
29. W.B. Dapp, A. Lücke, B.N.J. Persson, M.H. Müser, Phys. Rev. Lett. **108**, 244301 (2012).
30. J.H.H. Bongaerts, K. Fourtouni, J.R. Stokes, Tribol. Int. **40**, 1531 (2007).
31. N. Hosoda, S.N. Gorb, Proc. R. Soc. London, Ser. B **279**, 4236 (2012).
32. D.J. Crisp, W.H. Thorpe, Discuss. Faraday Soc. **3**, 210 (1948).
33. D. Neumann, D. Woermann, Naturwiss. **96**, 933 (2009).
34. G. McHale, M.R. Flynn, M.I. Newton, Soft Matter **7**, 10100 (2011).
35. A. Beskok, G.E. Karniadakis, Microscale Thermophys. Engin. **3**, 43 (1999).
36. Z.L. Guo, B.C. Shi, C.G. Zheng, EPL **80**, 24001 (2007).
37. Z.L. Guo, C.G. Zheng, B.C. Shi, Phys. Rev. E **77**, 036707 (2008).
38. V.K. Michalis, A.N. Kalarakis, E.D. Skouras, V.N. Burganos, Microfluid Nanofluid **9**, 847 (2010).
39. G.T. Roberts, J. Phys. A **2**, 685 (1969).